Electronic Supplementary Material (ESI) for Journal of Materials Chemistry A.

Supporting Information

Selenium-vacancies Rich $CoSe_2$ Ultrathin Nanomeshes with Abundant Active Sites for Electrocatalytic Oxygen Evolution

Yixin Zhang,[a, ‡] Chao Zhang,[a, ‡] Yamei Guo,[a, *] Dali Liu,[a] Yifu Yu,[a, *] and Bin Zhang[a, b]

[a] Tianjin Key Laboratory of Molecular Optoelectronic Sciences, Department of Chemistry, School of Science, Tianjin University, No. 135 Yaguan Road, Haihe Education Park, Jinnan District, Tianjin 300354, China

[b] Collaborative Innovation Center of Chemical Science and Engineering, No. 92 Weijin Road, Nankai District, Tianjin 300072, China

[*] Corresponding Author: bzhang@tju.edu.cn (B.Z.)

[‡] These authors contributed equally to this work.

1. Experimental Procedures

1.1 Materials Synthesis

1.1.1 Chemicals. Cobalt acetate ($Co(Ac)_2 \cdot 4H_2O$, 98%), diethylenetriamine (DETA, 99%), Potassium selenate (K_2SeO_3, 99%), cobalt powder (Co, 99.9%), Selenium powder (Se, 99.9%), ethanol (99.7%), KOH (90%) and Nafion solution (5 wt %) were purchased from Aladdin Ltd. (Shanghai, China). All chemicals are analytical grade and used as received without any further purification.

1.1.2 Synthesis of lamellar $CoSe_2$/DETA hybrid precursors. The lamellar $CoSe_2$/DETA hybrid precursors were synthesized according to the reported literature.[1] In a typical procedure, 1 mmol $Co(Ac)_2 \cdot 4H_2O$ and 1mmol K_2SeO_3 were dissolved in 26 mL deionized water under the condition of ice-water bath. Then, 13 mL diethylenetriamine (DETA) was dropwise added into the solution. After stirring for half an hour, the obtained solution was transferred into a 50 mL Teflon-lined autoclave and maintained at 180 °C for 16 h. The black floccules were collected after naturally cooling down to room temperature and then washed with absolute ethanol. Finally, the black products were obtained after drying under vacuum at 60 °C for 6 h.

1.1.3 Synthesis of $CoSe_2$ ultrathin nanomeshes with selenium vacancies ($CoSe_2$ UNM_{vac}). The $CoSe_2$/DETA hybrid precursors were put on the bottom of quartz boat and treated by Ar plasma (commercial 13.56 MHz RF source) for 20 min with power of 300 W, pressure of 70 Pa and gas flow rate of 200 mL min^{-1}. After half an hour, the sample was collected and washed with absolute ethanol for once. Finally, the product was obtained after drying under vacuum at 60 °C for 6 h.

1.1.4 Synthesis of $CoSe_2$ nanosheets ($CoSe_2$ NS). The $CoSe_2$ NS were obtained according to the reported literature by sonication treatment.[1] In a typical procedure, 20 mg $CoSe_2$/DETA hybrid precursors was dispersed into 50 mL ethanol. Then, the mixture was sonicated at 300 W for 12 h. The resultant dispersions were centrifuged at 2000 r.p.m. for 10 min and

the precipitate was thrown away to remove the non-exfoliated component. The sample was collected by centrifuging the suspension at 12000 r.p.m. for 10 min and washed with ethanol. Finally, the product was obtained after drying under vacuum at 60 °C for 6 h.

1.1.5 Synthesis of $CoSe_2$ nanoparticles ($CoSe_2$ NP). The $CoSe_2$ nanoparticles were prepared according to the previous literature[1]. In a typical procedure, stoichiometric cobalt powder and selenium powder were fully mixed and loaded in a fused silica tube. Hereafter, the mixture was heated at 650 °C for 12 h in a static Ar atmosphere with a heating rate of 2°C min^{-1} and cooled to room temperature. The final sample was washed with distilled water and ethanol for several times and dried under vacuum at 60 °C for 6 h.

1.2 Characterization

The scanning electron microscopy (SEM) images were taken with a Hitachi S-4800 scanning electron microscope. The transmission electron microscopy (TEM), high resolution transmission electron microscopy (HRTEM) images, and elemental distribution mapping images were carried out with a JEOL JEM-2100F microscope. The X-ray diffraction (XRD) patterns were carried out with a Panalytical X'Pert Pro diffraction system with a Cu Kα source (λ = 1.54056 Å). The thickness of nanosheets was determined by atomic force microscopy (AFM) (Bruker multimode 8). Fourier transform infrared spectroscopy (FT-IR) spectrum was carried out with a MAGNA1IR 750 (Nicolet Instrument Co) FTIR spectrometer. The electron paramagnetic resonance (EPR) spectra were recorded on a Bruker EMX-8 spectrometer operated at 9.45 GHz 100 K. The X-ray photoelectron spectroscopy (XPS) was recorded on Perkin Elmer PHI 1600 Versa Probe (Al Kα). All the peaks are calibrated with C 1s spectrum at binding energy of 284.8 eV.

1.3 *g*-factor in EPR.

The g-factor was calculated by the following formula.

$$g = \frac{h\upsilon}{\beta H}$$

β = 9.2710×10^{-21} erg·G^{-1}; h = 6.62620×10^{-27} erg·S; The electron paramagnetic resonance

(EPR) spectra were recorded on a Bruker EMX-8 spectrometer operated at 9.45 GHz 100 K, so υ = 9.45 GHz = 9.45×10^9 Hz; We can obtain the H from the Figure 2a, H = 3373.7 G. Therefore,

$$g = \frac{6.626\times10^{-27} erg\cdot S\times 9.45\times10^{9} Hz}{9.2710\times10^{-21} erg\cdot G^{-1}\times 3373.7G} = 2.0020558 \approx 2.002$$

1.4 Electrochemical measurements.

Electrochemical measurements were performed with a CHI 660D electrochemical workstation (CH Instruments, Austin, TX) and a typical three-electrode cell was used, including a working electrode, a Hg/HgO electrode (1.0 M KOH) as the reference electrode, and a glassy carbon counter electrode in 1.0 M KOH electrolyte. The electrolyte was degassed by bubbling O_2 for 30 min before the OER measurements. If without extra statement, all the mentioned potentials were against reversible hydrogen electrode (RHE). All the data in electrochemical section was *iR* corrected. A glassy carbon electrode decorated with catalyst samples was used as the working electrode. In a typical procedure of the fabrication of the working electrode, 4 mg of catalysts and 20 μL of 5% Nafion solution were dispersed in 1 mL deionized water by sonication to generate a homogeneous ink. Then 5 μL of the dispersion (containing 20 μg catalyst) was transferred onto a glassy carbon electrode of 3 mm in diameter (loading amount: 0.28 mg cm^{-2}). The as-prepared catalyst film was dried at room temperature. Polarization data were collected at a sweep rate of 5 mV s^{-1}.

1.5 Mass activity.

Mass activity (A g^{-1}) of different samples as shown in Figure 3c was calculated from the following equation.

$$Mass\ activity = \frac{j}{m}$$

where m is the loading amount of electrocatalyst, i.e. 0.28 mg cm^{-2}; *j* is the measured current density (mA cm^{-2}) at the overpotential of 200 mV, 250 mV, 300 mV and 350 mV.

1.6 The concentration of surface active sites from the redox features in cyclic voltammetry (Figure S5).

Calculated area for $CoSe_2$ UNM_{vac} associated with the reduction of Co^{3+} to Co^{2+} = 0.0004697 V · A

Hence, the surface concentration of Co for $CoSe_2$ UNM_{vac} that participated in OER = 0.0004697 V · A / (0.3 V S^{-1} × 1.602 × 10^{-19} C × 1)= 9.773 × 10^{15}.

In the same way, the surface concentration of Co for $CoSe_2$ NS = 0.0004632 V · A / (0.3 V S^{-1} × 1.602 × 10^{-19} C × 1) = 9.638 × 10^{15}.

The surface concentration of Co for $CoSe_2$ NP = 2.5019 × 10^{-5} V · A / (0.3 V S^{-1} × 1.602 × 10^{-19} C × 1) =5.205 × 10^{14}.

1.7 Determination of Turnover Frequency (TOF) from OER current density.

TOF in our study was calculated assuming that the surface active Co atoms in the redox reaction only participated in OER electrocatalysis. The following equation is,

$$TOF = \frac{j \times N_A}{z \times F \times \Gamma}$$

j stands for the current density (A cm^{-2}), N_A is the Avogadro number, z is the number of electrons transferred to evolve a molecule of product (for O_2, it is 4), F is the Faraday constant (96485 C mol^{-1}) and Γ is the surface concentration of active sites or number of participating atoms in the catalyst material.

Therefore,

$$TOF = \frac{j \times 6.023 \times 10^{23}}{4 \times 96485 \times \Gamma}$$

2. Results and Discussion

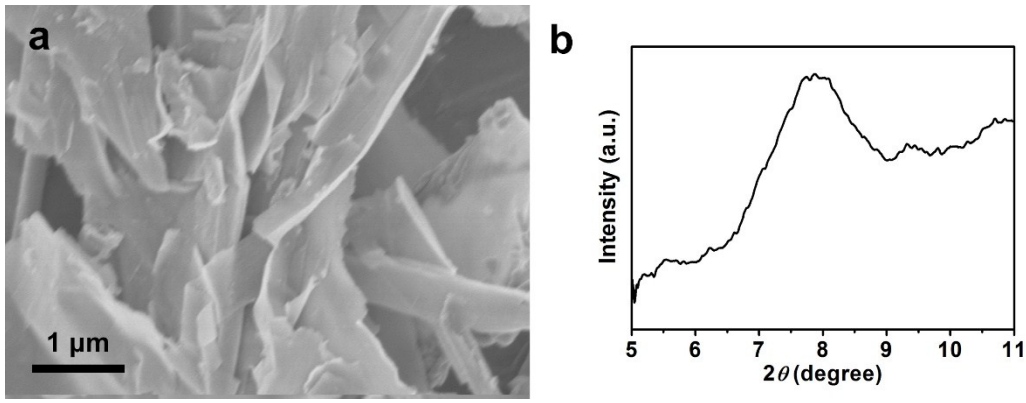

Fig. S1 Characterizations of $CoSe_2$/DETA hybrid precursors. (a) SEM image and (b) XRD pattern of lamellar $CoSe_2$/DETA hybrid precursors.

The SEM image (Fig. S1a) clearly shows the lamellar two-dimensional (2D) morphology of the as-prepared precursors. The XRD result (Fig. S1b) identifies the precursors as $CoSe_2$/DETA hybrids.

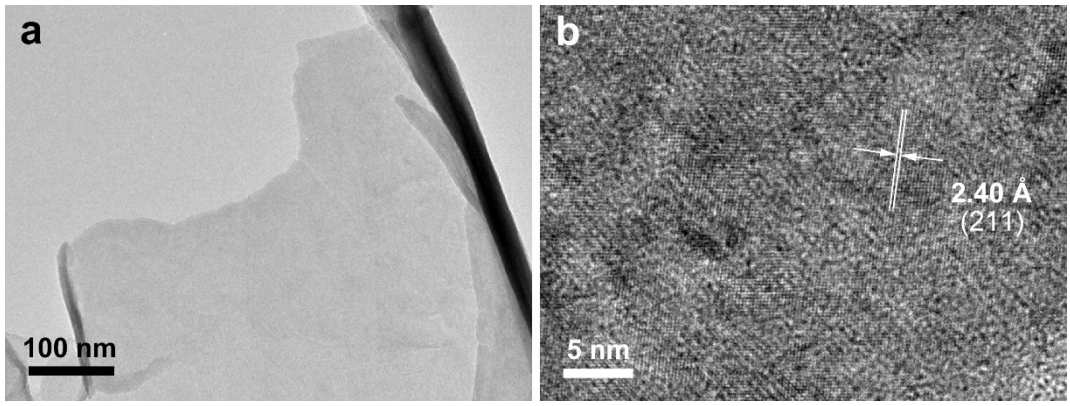

Fig. S2 Characterizations of $CoSe_2$ NS. (a) TEM image, and (b) HRTEM image of $CoSe_2$ NS.

After sonication treatment, the lamellar $CoSe_2$/DETA precursors are exfoliated into free-standing nanosheets as shown in TEM image (Fig. S2a). The HRTEM image (Fig. S2b) displays the lattice spacing of 2.40 Å, which is corresponding to (211) crystallographic plane of cubic $CoSe_2$, indicating the formation of $CoSe_2$ nanosheets ($CoSe_2$ NS).

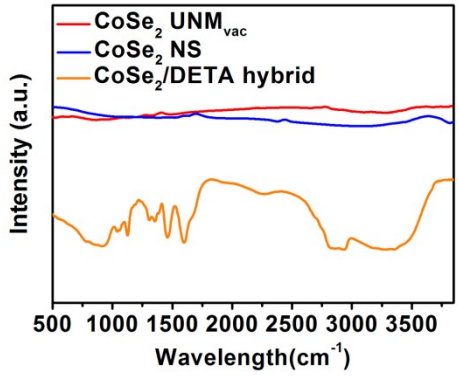

Fig. S3 FT-IR spectra of $CoSe_2$ UNM_{vac}, $CoSe_2$ NS and $CoSe_2$/DETA hybrid precursors.

The FT-IR adsorption peaks of organic group in $CoSe_2$/DETA hybrids become disappeared after exfoliation into $CoSe_2$ UNM_{vac} and $CoSe_2$ NS (Fig. S3). These results demonstrate that DETA is totally removed from lamellar $CoSe_2$/DETA hybrid precursors after the plasma and sonication treatment. The surface of as-obtained $CoSe_2$ UNM_{vac} and $CoSe_2$ NS is clean, which would be crucial for the following electrocatalytic measurements.

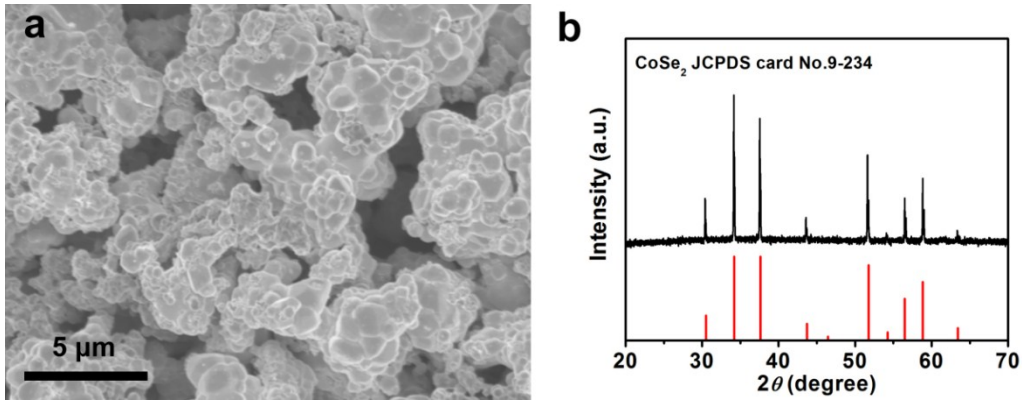

Fig. S4 Characterizations of $CoSe_2$ NP. (a) SEM image and (b) XRD pattern of $CoSe_2$ NP.

Table S1 Comparison of alkaline OER performance for $CoSe_2$ UNM_{vac} with other Co-based electrocatalysts.

Catalyst	Electrolyte	Mass loading (mg cm^{-2})	Overpotential (mV) η_{10}	Tafel slope (mV dec^{-1})	TOF (s^{-1}) η=300 mV	Ref.
$CoSe_2$ UNM_{vac}	**1 M KOH**	**0.28**	**284**	**46.3**	**2.47**	**This work**
$CoSe_2$ NS	**1 M KOH**	**0.28**	**343**	**97.7**	**0.51**	**This work**
$CoSe_2$ NP	**1 M KOH**	**0.28**	**466**	**111.1**	**0.39**	**This work**
α-$Co_4Fe(OH)_x$	1 M KOH	0.28	295	52	0.027	2
Co@NC	1 M KOH	0.32	390			3
Co_3O_4 mesoporous NTs	0.1 M KOH	0.208	390	76		4
Co_3O_4 nanowires	1 M KOH	0.136	403	72		5
Co_3O_4 NA/CF	1 M KOH	1.9		71	0.19 at η=350	6
Co-CN SS	1 M KOH	0.285	340	79		7
CoMn LDH	1 M KOH	0.142	324	43	0.075	8
Co-MOF/NF	1 M KOH	5.84		77	~0.013	9
CoP NPs	1 M KOH	0.71	340	99		10
Fe_xCo_y-ONSs	0.1 M KOH	0.36	308	36.8	0.022 at η=350	11
NiCo LDH	1 M KOH	0.07	~335	41	0.11	12
CoCo LDH	1 M KOH	0.07	~354	45	0.0035	12
NiCoP nanoboxes	1 M KOH	0.255	370	115		13
ultrathin porous Co_3O_4 nanoplates	0.1 M KOH	0.56	523	71	0.0042 at η=400	14

η_{10}: the overpotential corresponding to current density of 10 mA cm^{-2}.

Areas are blank if the corresponding data are not mentioned in references.

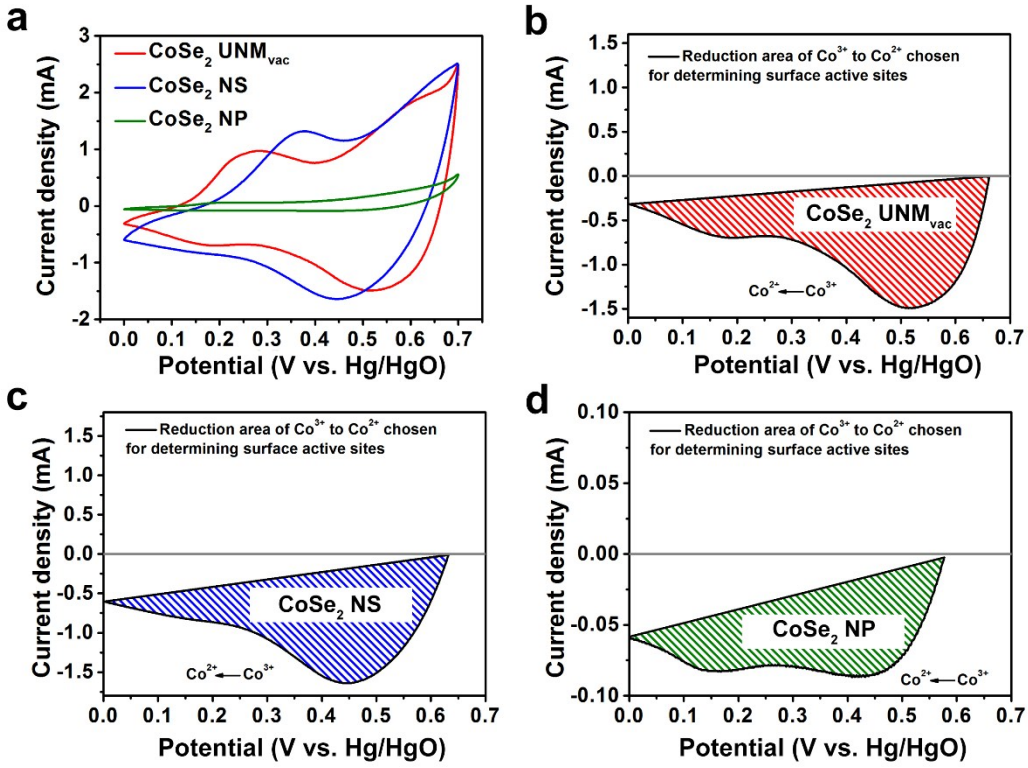

Fig. S5 (a) Cyclic voltammetry (CV) curves of $CoSe_2$ UNM_{vac}, $CoSe_2$ NS and $CoSe_2$ NP. (b-d) The area of redox features of different samples for the calculation of surface active sites.

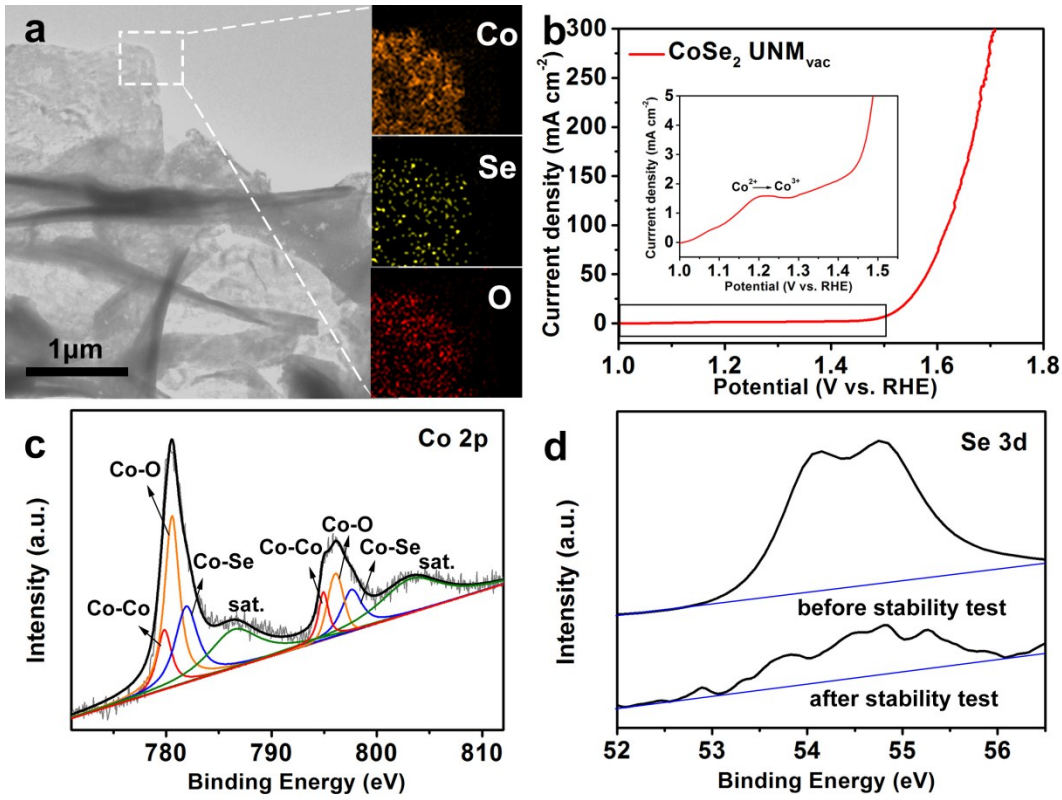

Fig. S6 Characterizations of $CoSe_2$ UNM_{vac} after stability test. (a) TEM image and STEM-EDS mapping images of $CoSe_2$ UNM_{vac} after stability test. (b) LSV curves of $CoSe_2$ UNM_{vac}. The inset is the magnification of black box of $CoSe_2$ UNM_{vac}.(c) Co 2p XPS spectra of $CoSe_2$ UNM_{vac} after stability test. (d) Se 3d XPS spectra of $CoSe_2$ UNM_{vac} before and after stability test.

$CoSe_2$ UNM_{vac} maintains the ultrathin nanomesh morphology after stability test (Fig. S6a). The appearance of oxygen element in mapping images after stability test reveals the transformation of $CoSe_2$ UNM_{vac} (Fig. S6a). The oxidation peak at ~1.22 V can be attributed to the redox couple of $Co^{2+/3+}$ (Fig. S6b), suggesting that the active species of $CoSe_2$ UNM_{vac} might be CoOOH, which is oxidized from $CoSe_2$. The Co-O peak at 780 eV in Co 2p XPS shows the formation of CoOOH in $CoSe_2$ UNM_{vac} after stability test (Fig. S6c). Moreover, Co-Se peak in Co 2p XPS (Fig. S6c) and the weak Se 3d peak (Fig. S6d) confirm the preservation of part $CoSe_2$ specie after stability test. All the results demonstrate that $CoSe_2$ UNM_{vac} is partly converted into CoOOH during the OER process.

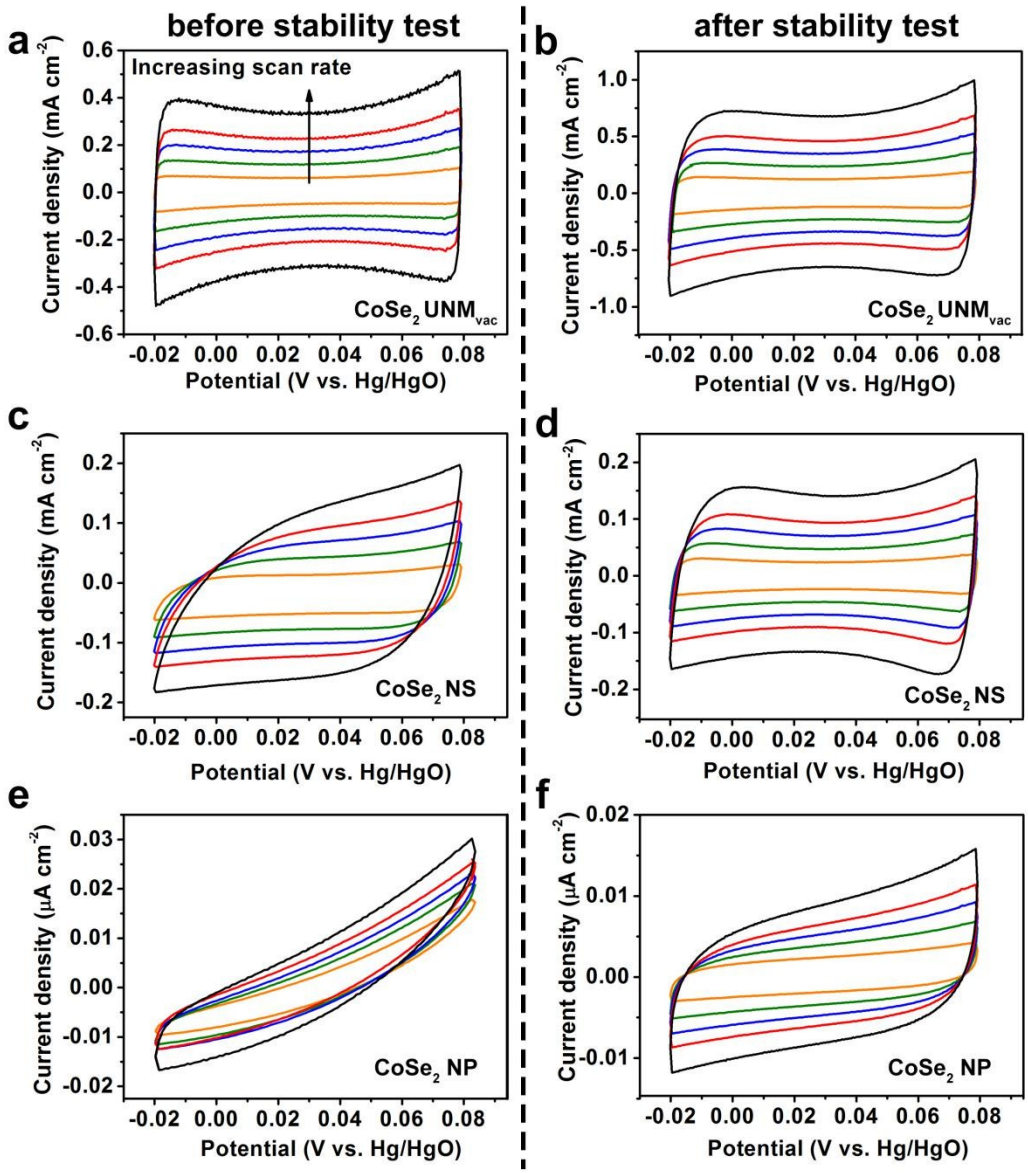

Fig. S7 Electrochemical capacitance measurements.

Electrochemical capacitance measurements were used to determine the electrochemical active surface areas (ECSA) of catalysts. To measure the electrochemical capacitance, the potential was swept between -0.02 and 0.08 V *vs.* Hg/HgO at different scan rates of 20, 40, 60, 80, 120 mV s^{-1}. We measured the capacitive currents at a potential where no faradic processes were observed, i.e. 0.03 V *vs.* Hg/HgO. The measured capacitive currents were plotted as a function of scan rate in Fig. S8 and a linear fitting determined the specific capacitance as 5.48 mF cm^{-2} for $CoSe_2$ UNM_{vac}, 1.18 mF cm^{-2} for $CoSe_2$ NS and 0.0645 mF cm^{-2} for $CoSe_2$ NP after the stability test. The specific capacitance for a flat surface is generally

found to be in the range of 20-60 μF cm^{-2}. In the following calculations of ECSA after stability test, we assume specific capacitance as 40 μF cm^{-2}.

$$A_{ECSA}^{CoSe_2UNM_{vac}} = \frac{5.48\,mF\,cm^{-2}}{40\,\mu F\,cm^{-2}\ per\ cm_{ECSA}^2} = 137\,cm_{ECSA}^2$$

$$A_{ECSA}^{CoSe_2NS} = \frac{1.18\,mF\,cm^{-2}}{40\,\mu F\,cm^{-2}\ per\ cm_{ECSA}^2} = 29.5\,cm_{ECSA}^2$$

$$A_{ECSA}^{CoSe_2NP} = \frac{0.0645\,mF\,cm^{-2}}{40\,\mu F\,cm^{-2}\ per\ cm_{ECSA}^2} = 1.61\,cm_{ECSA}^2$$

The larger ECSA value of $CoSe_2$ UNM_{vac} demonstrate that there are more active sites in $CoSe_2$ UNM_{vac} owing to the ultrathin nanomesh structure and the existence of selenium vacancies.

Moreover, the specific capacitance is 2.78 mF cm^{-2} for $CoSe_2$ UNM_{vac}, 1.05 mF cm^{-2} for $CoSe_2$ NS and 0.0626 mF cm^{-2} for $CoSe_2$ NP before stability test. Thus, the increment in ECSA for the samples before and after stability test,

$$\text{CoSe}_2\ \text{UNM}_{\text{vac}}:\ \frac{(5.48-2.78)mF\,cm^{-2}}{2.78\,mF\,cm^{-2}} = 97.12\,\%$$

$$\text{CoSe}_2\ \text{NS}:\ \frac{(1.18-1.05)mF\,cm^{-2}}{1.05\,mF\,cm^{-2}} = 12.38\,\%$$

$$\text{CoSe}_2\ \text{NP}:\ \frac{(0.0645-0.0626)mF\,cm^{-2}}{0.0626\,mF\,cm^{-2}} = 3.04\,\%$$

$CoSe_2$ UNM_{vac} have a maximum increment in ECSA with 97.12 % after the stability test, indicating that the ultrathin nanomesh structure and the existence of selenium vacancies would provide a huge increment of active sites in the oxygen evolution progress.

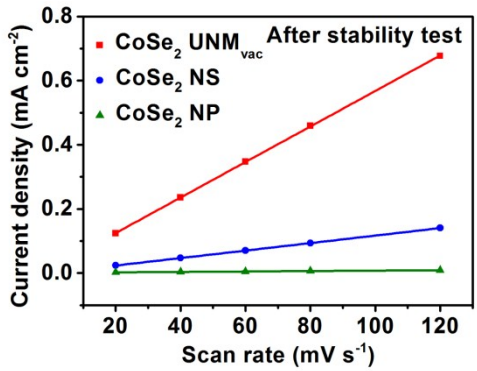

Fig. S8 Plots of the current density at 0.03 V vs scan rate for $CoSe_2$ UNM_{vac}, $CoSe_2$ NS and $CoSe_2$ NP after stability test.

Reference:

1 Liu, Y.; Cheng, H.; Lyu, M.; Fan, S.; Liu, Q.; Zhang, W.; Zhi, Y.; Wang, C.; Xiao, C.; Wei, S.; Ye, B. and Xie, Y., *J. Am. Chem. Soc.* 2014, **136**, 15670-15675.

2 Jin, H.; Mao, S.; Zhan, G.; Xu, F.; Bao, X. and Wang, Y., *J. Mater. Chem. A* 2017, **5**, 1078-1084.

3 Cui, X.; Ren, P.; Deng, D.; Deng, J. and Bao, X., *Energ. Environ. Sci*. 2016, **9**, 123-129.

4 Wang, H.; Zhuo, S.; Liang, Y.; Han, X. and Zhang, B., *Angew. Chem. Int. Ed*. 2016, **55**, 9055-9059.

5 Wang, Y.; Zhou, T.; Jiang, K.; Da, P.; Peng, Z.; Tang, J.; Kong, B.; Cai, W.-B.; Yang, Z. and Zheng, G., *Adv. Energy Mater*. 2014, **4**, 1400696.

6 Wei, Y.; Ren, X.; Ma, H.; Sun, X.; Zhang, Y.; Kuang, X.; Yan, T.; Ju, H.; Wu, D. and Wei, Q., *Chem. Commun*. 2018, **54**, 1533-1536.

7 Shi, Y.; Wang, Y.; Yu, Y.; Niu, Z. and Zhang, B., *J. Mater. Chem. A* 2017, **5**, 8897-8902.

8 Song, F. and Hu, X., *J. Am. Chem. Soc*. 2014, **136**, 16481-16484.

9 Zhang, X.; Sun, W.; Du, H.; Kong, R.-M. and Qu, F., *Inorg. Chem. Front*. 2018, **5**, 344-347.

10 Chang, J.; Xiao, Y.; Xiao, M.; Ge, J.; Liu, C. and Xing, W., *ACS Catal*. 2015, **5**, 6874-6878.

11 Zhuang, L.; Ge, L.; Yang, Y.; Li, M.; Jia, Y.; Yao, X. and Zhu, Z., *Adv. Mater*. 2017, **29**, 1606793.

12 Song, F. and Hu, X., *Nat. Commun*. 2014, **5**, 4477.

13 He, P.; Yu, X. Y. and Lou, X. W., *Angew. Chem. Int. Ed*. 2017, **56**, 3897-3900.

14 Zhou, X.; Xia, Z.; Tian, Z.; Ma, Y. and Qu, Y., *J. Mater. Chem. A* 2015, **3**, 8107-8114.